Available online at www.sciencedirect.com
SCIENCE DIRECT
International Journal of Heat and Fluid Flow 27 (2006) 534–541
International Journal of HEAT AND FLUID FLOW
www.elsevier.com/locate/ijhff

Length and time scales of the near-surface axial velocity in a high Reynolds number turbulent boundary layer

M. Metzger *

Department of Mechanical Engineering, University of Utah, 50 S. Central Campus Dr., Rm 2110, Salt Lake City, UT 84112, United States

Abstract

Reynolds number effects on relevant length and time scales in the near-wall region of a canonical turbulent boundary layer are investigated. Well resolved measurements in the atmospheric surface layer are compared with existing laboratory data to give a composite Reynolds number range spanning over three orders of magnitude. In the field experiments, a vertical rake of twenty single element hot-wires was used to measure the axial velocity, u, characteristics in the lower log layer region of the atmospheric surface layer that flows over Utah's western desert. Only data acquired under conditions of near-neutral thermal stability are analyzed. The shape of the power spectra of u as a function of distance from the wall, y, and Reynolds number is investigated, with emphasis on the appropriate scaling parameters valid across different wavenumber, k, bands. In particular, distance from the wall is found to scale the region of the u spectra around $ky = 1$. The presence of a k^{-1} slope in the spectra is also found to correlate with the Reynolds number dependence in the peak of the root mean square u profile. In addition, Reynolds number trends in the profiles of the Taylor microscales, which represent intermediate length and time scales in the boundary layer, are shown to deviate from classical scaling.

Keywords: Turbulent boundary layer; Atmospheric boundary layer

1. Introduction

The canonical turbulent boundary layer (TBL) is of fundamental interest because it provides a basis for understanding more complicated flows. Almost all practical applications involving TBLs are characterized by high Reynolds numbers, including, for example, airfoils and submarine hulls. Due to limitations in computational and experimental resources, most numerical and laboratory model studies are conducted at much low Reynolds numbers. Results from these model studies can only be effectively extrapolated to higher, more practical Reynolds numbers, if the appropriate TBL scaling parameters and relations are known. Currently, such scaling behaviors remain largely indeterminate, for both canonical and non-canonical TBLs.

The present study aims to address this issue by probing a naturally high Reynolds number turbulent boundary, namely the atmospheric boundary layer (ABL), and comparing to laboratory data obtained at much lower Reynolds numbers. In both cases, good spatiotemporal resolution of the measurement technique is maintained to avoid contamination of the results by spatial averaging, which tends to mask true Reynolds number effects, see Metzger and Klewicki (2001) for further discussion. The unique aspects of the present study, i.e., the good spatial resolution over a sufficiently large Reynolds number range (three orders of magnitude), therefore, are significant with respect to ascertaining potential scaling relations.

2. Experimental set-up

Hot-wire anemometry experiments were performed at the surface layer turbulence and environmental science test (SLTEST) facility on the salt playa of Utah's western

* Tel.: +1 801 581 5032; fax: +1 801 585 0039.
E-mail address: m.metzger@utah.edu

0142-727X/$ - see front matter © 2006 Elsevier Inc. All rights reserved.
doi:10.1016/j.ijheatfluidflow.2006.02.021

desert under conditions of near-neutral thermal stability. The SLTEST site is particularly suitable for high Reynolds number (based on momentum thickness, $R_\theta \approx 5 \times 10^6$) canonical TBL studies due to the sparsity of vegetation, the smooth flat surface (aerodynamic roughness length, $z_0 \approx 0.5$ mm), and the relatively predictable diurnal wind patterns resident in the early summer. Attributes of the site are described in further detail by Metzger (2002). In the present study, a tower of 20 simultaneously sampled hot-wires (shown in Fig. 1) was used to interrogate the turbulent axial velocity in the near-surface region spanning $5 \leqslant y^+ \leqslant 10^4$, where y denotes the distance from the surface. Note, the superscript + indicates inner normalization by kinematic viscosity, ν, and friction velocity, $u_\tau (\equiv \sqrt{\tau_w/\rho})$, where τ_w and ρ denote the wall shear stress and air density, respectively. Because of inherent temporal variations in the atmosphere, simultaneous data are needed to clarify trends in the statistical profiles. Therefore, the tower of simultaneously sampled velocity measurements represents an essential feature of the present study over previous studies.

The present hot-wire data are accompanied by coincident meteorological data, including three-dimensional velocity from sonic anemometers located at 2, 3, and 5 m above the surface, direct surface shear stress from a floating-element drag plate, mean velocity profiles up to 150 m from a minisodar, net surface radiation, and surface temperature gradient measurements. In order to deduce Reynolds number effects on the structure of the TBL, the present atmospheric results are compared with wind tunnel data acquired in the range $2500 \leqslant R_\theta \leqslant 5 \times 10^3$. In all cases, the inner normalized wire length is less than 10, yielding good spatial resolution over three orders of magnitude in Reynolds number.

Fig. 1. Photograph of the hot-wire experiment at the SLTEST site in Utah's western desert. Twenty hot-wires are spaced nearly logarithmically, spanning an overall distance of 1 m above the surface.

3. Challenges with atmospheric boundary layer experiments

The challenges of performing hot-wire experiments in the atmospheric surface layer are multifaceted. On a practical level, field trials are physically demanding and require special facilities for on-site hot-wire calibration, which must be performed frequently. Calibration algorithms must also explicitly incorporate temperature compensation (Metzger and Klewicki, 2003) since ambient air temperature changes dramatically over the course of the day. Since hot-wire probes are directionally sensitive, i.e., data may become contaminated by substantial crosswinds, care must be taken to constantly align the probes with the mean wind direction. In addition, field trials can be costly and risky, in the sense that the potential for instrumentation and sensor damage, due to, for example, environmental factors such as dust and high speed winds, are much greater than typical laboratory studies.

On a more technical level, the ABL differs from the canonical laboratory generated boundary layer, aside from the Reynolds number difference, in two important ways: (i) the ABL is not statistically stationary and (ii) the ABL is thermally stratified. The former poses challenges in determining the appropriate averaging time to use in calculating the vertical momentum flux, for example, which is typically used in atmospheric studies to estimate the local friction velocity. A method of determining a critical averaging time for computing atmospheric fluxes has recently been proposed (Holmes and Metzger, 2005) and may prove helpful in this regard. The second difference results from the diurnal heating and cooling of the Earth's surface, which leads to the inherent thermal stratification of the atmosphere. During the transitions between heating and cooling (sunrise and sunset), the atmospheric boundary layer passes through neutral stability whereby boundary layer turbulence is driven predominantly via mechanical shear, with buoyancy effects being negligible. Therefore, in order to make direct comparisons between ABL data and wind tunnel measurements, only field data acquired during conditions of near-neutral thermal stability are considered. This poses definite challenges with respect to measuring the thermal stability and performing thorough checks on data quality to ensure that thermal effects are not influencing observed trends in the results. Work in progress by the author aims to address this issue, as well.

4. Axial velocity results

4.1. Statistical profiles

Fig. 2 presents the inner normalized mean axial velocity profiles from several atmospheric studies, including that of Metzger and Klewicki (2001), Metzger et al. (2001), and Folz (1997). All data exhibit a logarithmic region with a slope similar to that observed at lower R_θ. Log laws derived using parameters from Coles (1969) and Osterlund et al. (2000) are shown for comparison. The present study only considers data where the surface may be considered relatively smooth, i.e., in terms of the inner normalized equivalent sand grain roughness, $k_s^+ \lesssim 25$.

Two factors play into the variability of k_s^+ at the SLTEST site. Atmospheric data during neutral stability indicate that, for a given surface condition, the friction velocity varies linearly with the mean wind speed at a height of about 2 m above the surface, $u_\tau \propto \overline{U}_{2\,\mathrm{m}}$, (see Metzger (2002) for further details). Thus, for a fixed k_s, as the mean wind speed increases, k_s^+ increases proportionally. In addition, over the course of the summer, the integrity of the desert surface degrades due to moisture depletion, causing a noticeable increase in the dimensional surface roughness by late summer. The former effect dominated in the 2003 data, shown in Fig. 2, which represents a composite of hot-wire, sonic anemometer, and minisodar measurements. As evident by the data, the surface condition affects the mean wind profile through the entire depth of the surface layer, estimated to be $\delta^+ \approx 8.5 \times 10^5$, the location at which the mean profile begins to deviate from the log law.

The inner normalized root mean square (rms) axial velocity profiles presented in Fig. 3, on the other hand, reveal distinct Reynolds number trends. Compared are the data of Metzger and Klewicki (2001), Folz (1997), DeGraaff and Eaton (2000), and Klewicki and Falco (1990), along with the prediction based on the scaling relation of Marusic et al. (1997). Of particular interest is understanding the proper scaling relation valid near the peak at $y^+ = 15$, since this corresponds, at least from low Reynolds number data, to the peak in the turbulent kinetic energy production. Renormalization using the mixed velocity scale of DeGraaff and Eaton (2000), i.e., $\sqrt{u_\tau U_\infty}$, appears to remove the observed Reynolds number trend near the peak at $y^+ = 15$. Interestingly, the mixed velocity scale represents the geometric mean between the smallest and largest velocity scales in the flow, and as such characterizes an intermediate velocity scale. Note, both a substantial Reynolds number range and sufficient spatial resolution are required to observe the Reynolds number behavior in Fig. 3. The present data are inconclusive, however, regarding a potential secondary peak near $y^+ = 550$ at $R_\theta \approx 5 \times 10^6$. Work in progress by the author aims to address this issue, as well as investigate possible scaling relations for the region of the profile between $40 < y^+ < 0.1\delta^+$. Note,

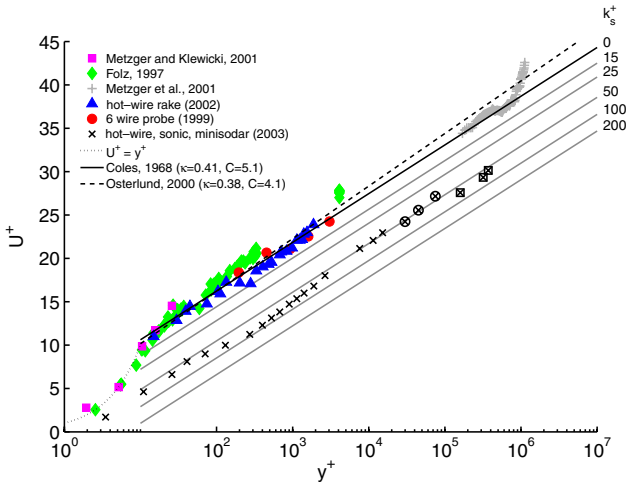

Fig. 2. Inner normalized mean axial velocity profile from atmospheric data obtained at SLTEST. The set of grey lines indicates the expected log law for different surface roughness, as parameterized by k_s^+.

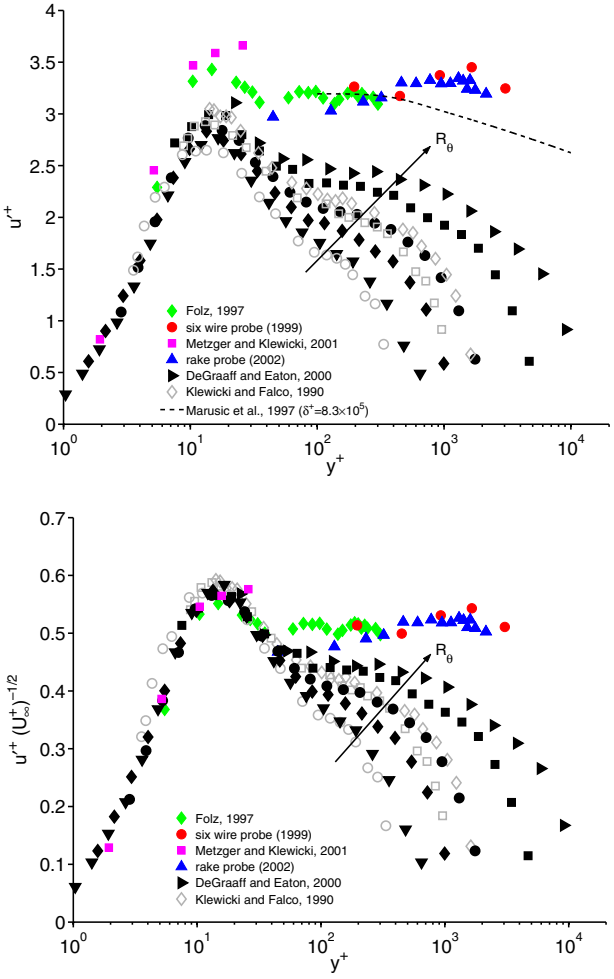

Fig. 3. Root mean square axial velocity profiles as a function of Reynolds number. Inner normalization (top) and mixed scaling (bottom). The arrows indicate the direction of increasing Reynolds number. The black solid and open grey symbols are from DeGraaff and Eaton (2000) and Klewicki and Falco (1990), respectively. All other symbols represent atmospheric data acquired at the SLTEST site.

the previous work of DeGraaff and Eaton (2000) showed that outer scaling is appropriate for $y^+ > 0.1\delta^+$.

4.2. Further support for mixed scaling near the peak

Mixed scaling of u' near the peak at $y^+ = 15$ implies

$$\frac{u'_{\max}}{(u_\tau U_\infty)^{1/2}} = C, \tag{1}$$

where C is a constant, independent of R_θ. Based on the data presented in Fig. 3, $C \approx 0.57$. Rearranging (1) yields

$$u'^{+}_{\max} = C\left(\frac{u_\tau}{U_\infty}\right)^{-1/2}. \tag{2}$$

On the other hand, a compilation of the current literature (see Metzger and Klewicki, 2001) suggests that

$$u'^{+}_{\max} = A\log(R_\theta) + B, \tag{3}$$

where $A = 0.22$–0.29 and $B = 1.84$–2.02 are empirical constants derived from a curve fit to the available data.[1] In order for both (2) and (3) to be valid concurrently, it is clear that the following must hold:

$$\left(\frac{u_\tau}{U_\infty}\right)^{-1/2} = a_1\log(R_\theta) + a_2, \tag{4}$$

where $a_1 = A/C = 0.39$–0.51 and $a_2 = B/C = 3.22$–3.54.

The quantity on the left hand side of (4) is relatively easy to measure in the Superpipe, since u_τ may be determined by the pressure drop along the pipe and U_∞ is simply the centerline velocity. The momentum deficit thickness, θ, is obtained by integrating the mean velocity profile across the boundary layer. Relatively minor uncertainties in the estimate of θ exist due to limitations in the measurement technique very near the pipe wall. Fig. 4 shows $(U^+_\infty)^{1/2}$ as a function of Reynolds number based on data from the study of McKeon et al. (2004). A curve fit through the data produces the following relation:

$$\left(\frac{u_\tau}{U_\infty}\right)^{-1/2} = 0.48\log(R_\theta) + 3.27. \tag{5}$$

The empirical coefficients in (5) fall directly within the range of a_1 and a_2 given above for (4).

Although the Superpipe data in Fig. 4 appear to exhibit a slight curvature when plotted semilogarithmically versus R_θ, the relation in (5) represents a very good first-order approximation. In this manner, the present analysis of Superpipe data provides strong independent support for the mixed scaling of u' near the peak. It does not, however, answer the question why U_∞ is an important velocity scale so close to the wall. Metzger and Klewicki (2001) showed that an increased contribution from low frequency motions at high Reynolds number underlies the observed rise in the peak of u'^{+} near $y^+ = 15$. This supposed modulation of u' by the freestream, becoming more pronounced with increasing Reynolds number, was anticipated by Bradshaw (1967). Nevertheless, a physical or mechanistic justification for this remains to be determined.

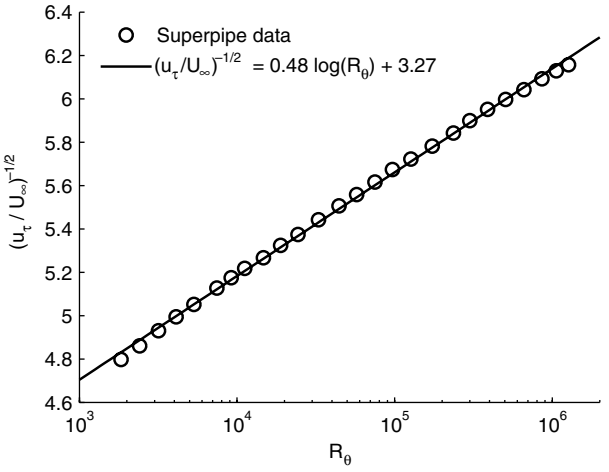

Fig. 4. Reynolds number dependence of the intermediate velocity scale, as based on Superpipe data of McKeon et al. (2004).

4.3. Spectra

En route to addressing the question put forward at the end of the previous section, it is helpful to investigate the spectra of u in some detail. Of particular interest is understanding the predominant time scales of the turbulent motions contributing to the overall axial velocity variance, and how these contributions vary with both distance from the surface and Reynolds number. Fig. 5 compares the premultiplied spectra of u at $y^+ \approx 15$ for Reynolds numbers

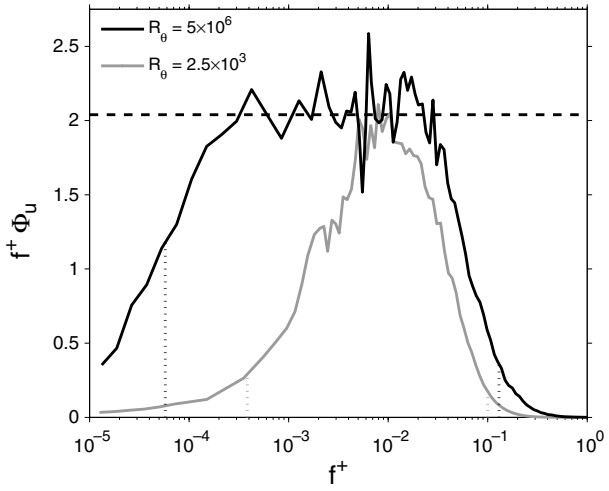

Fig. 5. Comparison of premultiplied spectra at $y^+ = 15$ for high and low R_θ. The dotted lines mark the approximate locations of the inverse Taylor and integral time scales for each data set. The black dashed line indicates a slope of -1, as would appear in the non-premultiplied spectra.

[1] An essential part of the analysis by Metzger and Klewicki (2001) is that only high resolution data, with sensor lengths less than or equal to 10 viscous units, were used in the curve fit.

$R_\theta = 5\times10^6$ (SLTEST) and $R_\theta = 2500$ (wind tunnel). Spectra are normalized such that the area under the curve is equal to the variance. Clearly, the high Reynolds number data exhibit an extended region with a -1 slope; while the low Reynolds number data show a much narrower frequency band with -1 slope. This is consistent with the result regarding the logarithmic Reynolds number dependence of the peak in u'^+ at $y^+ \approx 15$, as described below.

4.3.1. Ramifications of a −1 slope

From the definition of the spectra,

$$u'^2 = \int_0^\infty \Phi_u \, \mathrm{d}f. \tag{6}$$

As apparent in Fig. 5, the predominant energy containing region of the spectra lies within the frequency band having a -1 slope, especially so at higher Reynolds number. Therefore, integrating the spectra over this frequency band yields a good estimate of the overall variance of u, i.e.,

$$u'^2 \approx \int_{\lambda_t^{-1}}^{T^{-1}} f^{-1} \, \mathrm{d}f, \tag{7}$$

where λ_t and T mark the approximate lower and upper bounds of the -1 slope region, as indicated by the dotted lines in Fig. 5. Physically, λ_t and T represent the Taylor microscale and integral time scales, respectively, which provide a measure of the characteristic intermediate and longest time scales in the flow. Performing the integration gives

$$u'^2 = \log(T^{-1}) - \log(\lambda_t^{-1}), \tag{8}$$

or

$$u'^2 = \log\left(\frac{\lambda_t}{T}\right). \tag{9}$$

The ratio of the time scales may be related to the Reynolds number (Tennekes and Lumley, 1972) yielding

$$u'^2 \propto \log(R_\theta). \tag{10}$$

The statement in (10) agrees qualitatively with the observation expressed by (3). This gives some physical justification tying the Reynolds number dependence in the peak of u'^+ to an extended region of -1 slope in the corresponding spectra that increases logarithmically with increasing R_θ. A similar connection was made in the work of Perry and Abell (1977). The basis for that connection, however, stems from the attached-eddy hypothesis of Townsend (1976) valid in the overlap region, $y^+ > 100$ and $y/\delta < 0.1$, and is much different than the observations made in the present study of a k^{-1} slope in the near-wall region ($y^+ \lessapprox 100$).

4.3.2. Distance from the wall effect

Scaling of the spectra at y^+ values further from the surface, relative to the peak in u'^+, were investigated to determine the extent of the -1 slope region for $y^+ > 15$. Fig. 6 shows the premultiplied spectra of the axial velocity at

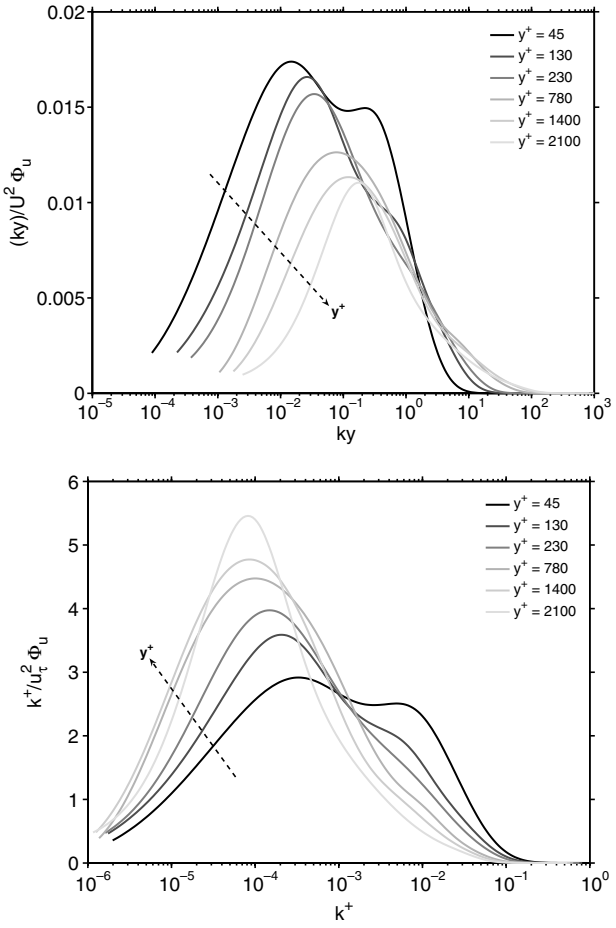

Fig. 6. Spectra of the axial velocity as a function of distance from the surface at $R_\theta \approx 5\times10^6$. Normalization with distance from the surface (top) and inner normalization (bottom). The dashed arrow indicates the direction of increasing y^+.

$R_\theta \approx 5\times10^6$ only, using both inner normalization and normalization by distance from the surface. In these plots k denotes the wavenumber, i.e., $k = 2\pi f/U$ where U represents an appropriate convection velocity dependent on y. Due to the scatter in the raw spectra at low wavenumber, some form of smoothing is necessary in order to ascertain trends in the results. Therefore, in the present study, raw premultiplied spectra were smoothed using a least squares spline approximation of fifth-order. The knot sequence of the spline was adjusted to minimize the total error, defined as the sum of the squared difference between the data and the spline fit, see Dierckx (1993).

The results in Fig. 6 indicate that for $y^+ > 45$, distance from the surface scales the spectra within a wavenumber band around $ky = 1$. An inherent feature of scaling with distance from the surface is that the overall range of scaled wavenumbers contributing to the variance decreases, i.e., the scaled spectra becomes compressed, in some sense, along the abscissa as y increases. Since the present data are limited to $y^+ = 2100$, the extent to which scaling with distance from the surface applies for larger y^+ remains to be seen.

Also evident in Fig. 6 is that the spectra at $y^+ = 45$ exhibits a much narrower region of k^{-1} slope, compared to that observed at $y^+ \approx 15$; while, spectra for $y^+ \geqslant 130$ do not possess a k^{-1} slope at all. This is consistent with the arguments presented earlier, see (10), that a k^{-1} slope in the spectra of u at any given y^+ corresponds to a logarithmic Reynolds number dependence in the variance of u at that same y^+. The logarithmic Reynolds number dependence of u' at $y^+ \approx 15$, in turn, corroborates the proposed mixed scaling of u' in this same region, as described in (1)–(5). Therefore, the lack of a k^{-1} slope in the high Reynolds number u spectra for $y^+ > 45$ is not inconsistent with the fact that mixed scaling ceases to be valid at this Reynolds number for $y^+ > 45$.

At lower Reynolds numbers, the u spectra typically displays a k^{-1} slope out to much higher y^+ (Perry and Abell, 1975). In fact, the scaling arguments of (Perry and Abell, 1977) predict a k^{-1} slope in the u spectra across the entire overlap region, i.e., $y^+ > 100$ and $y/\delta < 0.1$, which is much different than the present observation of a k^{-1} slope in the spectra at $y^+ \approx 15$. One plausible reason for this discrepancy stems from the rms profile (see Fig. 3). At lower R_θ, mixed scaling appears to extend out to a much higher y^+, relative to δ^+; as R_θ increases, the u' profiles peel away from the mixed scaling line at ever decreasing y^+, approaching the location of the peak near $y^+ = 15$. For example, at the lowest Reynolds number ($R_\theta \approx 1500$), mixed scaling appears to be valid out to $y^+ \approx 100$, or equivalently $y/\delta \approx 0.1$. At $R_\theta \approx 5 \times 10^6$, however, mixed scaling ceases to be valid for $y^+ > 45$, which is a substantially smaller fraction of δ at this high Reynolds number. Based on the observed correlation, described herein, between mixed scaling in the u' profile and the existence of a k^{-1} region in the spectra, it is not surprising that as R_θ increases, the k^{-1} region in the u spectra becomes less pronounced, and even disappears, for y^+ positions increasing beyond the peak location in u'.

4.4. Taylor microscales

Previous studies indicate that the Taylor microscale plays a significant role in scaling turbulent bursting frequencies, event durations, spectra, and statistics (Klewicki and Falco, 1996; Metzger et al., 2003; Nagano et al., 1998). Because of the potential relevance toward understanding momentum and scalar transport across the TBL, deciphering the scaling properties of the Taylor time and length scales is believed to be important. Toward this end, the present study considers the variation of the Taylor microscale (both length and time) as a function of R_θ and y.

The Taylor length scale, λ, represents a characteristic length associated with the ratio of the dissipation of turbulent kinetic energy, ϵ, and the turbulent kinetic energy, itself. As such, λ represents an intermediate scale between the inner (u_τ/ν) and outer (δ) length scales. Assuming isotropic turbulence, see Tennekes and Lumley (1972),

$$\epsilon = 15\nu\left\langle\left(\frac{\partial u}{\partial x}\right)^2\right\rangle \sim 15\nu\frac{\langle u^2\rangle}{\lambda^2}, \tag{11}$$

where $\langle\cdot\rangle$ denotes an appropriate time average. Therefore, the Taylor length scale is estimated from experimental data using the relation

$$\lambda^2 = \frac{\langle u^2\rangle}{\left\langle(\partial u/\partial x)^2\right\rangle}. \tag{12}$$

The present study utilizes Taylor's frozen turbulence hypothesis along with a Savitzky–Golay filter to evaluate the derivative in (12). The Taylor time scale, λ_t, is calculated in a more straightforward manner using an osculating parabola fit to the autocorrelation of u at zero time lag. Therefore, calculation of λ_t does not rely on the assumption of isotropy. The inner normalized results are plotted in Fig. 7. Importantly, the high Reynolds number atmospheric data shown were acquired over three different years with varying hot-wire probe types; yet, all of the results agree well.

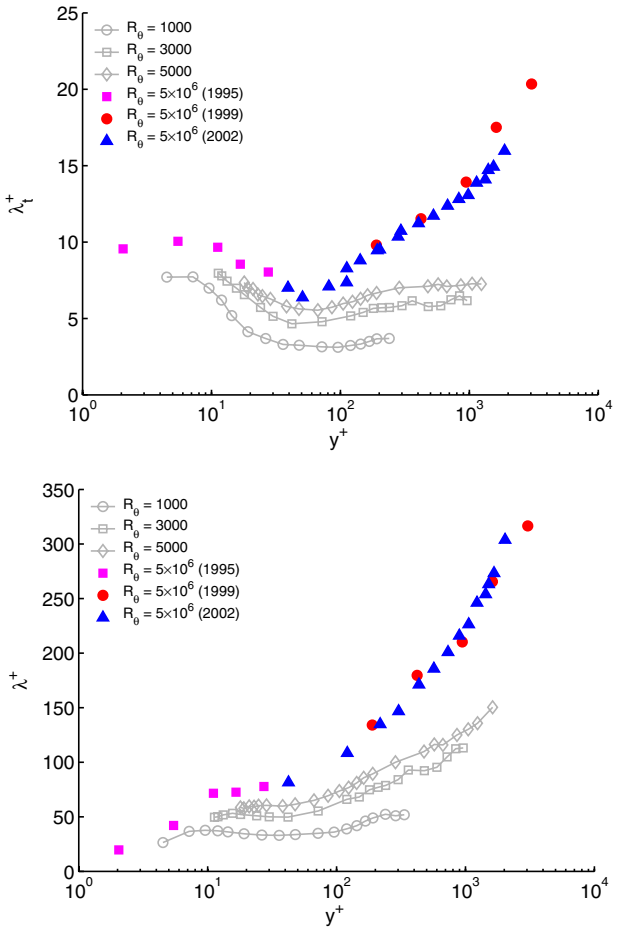

Fig. 7. Inner normalized Taylor microscale as a function of distance from the surface and Reynolds number. Taylor time scale (top) and Taylor length scale (bottom). The open symbols were calculated from the data of Klewicki (1989). The solid symbols represent data acquired at the SLTEST site.

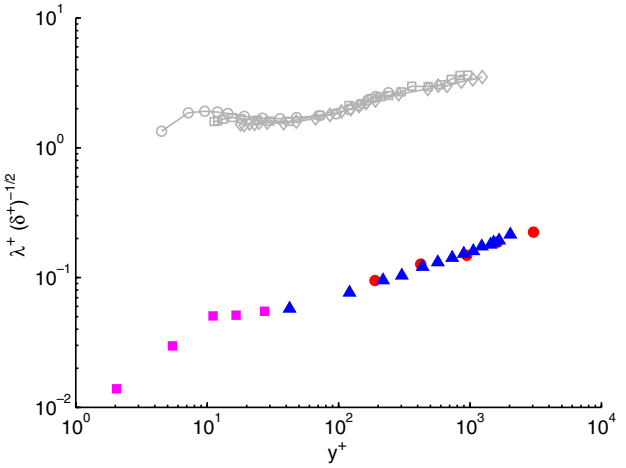

Fig. 8. Classical scaling of the Taylor length scale. Symbols are the same as that in Fig. 7.

Clearly, inner normalization is not the appropriate scaling measure for the Taylor microscale. Classical scaling arguments (Tennekes and Lumley, 1972, p. 67), based on the assumption that energy dissipation equals production, predict that

$$\frac{\lambda}{\delta} \sim (R_\delta)^{-1/2}, \tag{13}$$

where $R_\delta = \tilde{u}\delta/\nu$ and $\tilde{u} \equiv \langle u^2 \rangle^{1/2}$. The relation in (13) may be rewritten as

$$\lambda^+ \sim (\delta^+)^{1/2} (\tilde{u}^+)^{-1/2}. \tag{14}$$

Fig. 8 presents the data from Fig. 7 rescaled using the relation in (14), without the $\tilde{u}^+$ factor, which is much smaller than δ^+. The data clearly deviate from classical scaling. Although the assumption of isotropy results in some uncertainty in the calculated values of λ, the author believes that this alone cannot account for the observed discrepancy in the high and low R_θ data shown in Fig. 8. Note, the difference in the values of the scaled λ is between one and two orders of magnitude. The sensitivity of the Taylor microscale to the assumption of isotropy clearly requires further investigation. Additional data is required to fill the Reynolds number gap between the present wind tunnel data and atmospheric measurements. This, however, is not a trivial task owing to the large demands on spatiotemporal resolution of the measurement technique in order to accurately obtain λ.

5. Summary

Under nearly ideal conditions, the atmospheric boundary layer at the SLTEST site comes close to mimicking the flow expected in a very large wind tunnel, and, until recently, has remained an untapped resource in the study of fundamental TBL physics. Because no other facility exists that can generate TBLs with Reynolds numbers as high as those encountered in the atmosphere, without putting severe demands on the spatial resolution of current measurement technology, it seems rational to seek answers to Reynolds number scaling relations by probing the atmosphere.

The present study compares atmospheric measurements of the axial velocity statistics, spectra, and Taylor microscale with corresponding laboratory data to address some of the open issues in boundary layer scaling. Further support of mixed scaling of the u' profile near the peak at $y^+ = 15$ was provided using independent mean velocity data from the Superpipe. Mixed scaling was also tied to the observation that the k^{-1} region in the u spectra at $y^+ \approx 15$ extends further into the low wavenumber regime at high R_θ, indicating that the increase in the peak value of u' results from an increased contribution at low wavenumbers. In addition, the k^{-1} region becomes less pronounced at high R_θ for $y^+ > 15$ and disappears altogether for $y^+ > 45$. This location corresponds roughly to the same y^+ location at which mixed scaling ceases to be valid in the u' profile. Finally, classical scaling arguments were shown to be inadequate in removing actual Reynolds number trends in the Taylor length scale. Further well resolved turbulence measurements at Reynolds numbers based on momentum thickness in the range 1×10^4–1×10^5 are needed to corroborate these observations.

Acknowledgements

This work was supported by NSF (grant monitor, M. Plesniak) and ONR (grant monitor, R. Joslin). The author gratefully acknowledges Drs. A. Smits and B. McKeon for providing the Superpipe data, Dr. J. Klewicki for providing wind tunnel data, and Mr. I. Atzet for assisting with the field trials.

References

Bradshaw, P., 1967. 'Inactive' motion and pressure fluctuations in turbulent boundary layers. Journal of Fluid Mechanics 30, 241–258.

Coles, D., 1969. Turbulent boundary layers in pressure gradients: A survey lecture. In: Coles, D., Hirst, H. (Eds.), Proceedings of the 1968 AFOSR-IFP–Stanford Conference on Computation of Turbulent Boundary Layers. Stanford University, Stanford, California.

DeGraaff, D., Eaton, J., 2000. Reynolds-number scaling of the flat plate turbulent boundary layer. Journal of Fluid Mechanics 422, 319–346.

Dierckx, P., 1993. Curve and surface fittings with splines. Oxford University Press, New York.

Folz, A.B., 1997. An experimental study of the near-surface turbulence in the atmospheric boundary layer. Ph.D. thesis, University of Maryland, College Park, Maryland.

Holmes, H., Metzger, M., 2005. Critical averaging time for atmospheric boundary layer fluxes. Bulletin of the American Physical Society, Division of Fluid Dynamics, November 20–22, vol. 50, Chicago, IL.

Klewicki, J., 1989. On the interactions between the inner and outer region motions in turbulent boundary layers. Ph.D. thesis, Michigan State University, East Lansing, Michigan.

Klewicki, J.C., Falco, R.E., 1990. On accurately measuring statistics associated with small-scales in turbulent boundary layers using hot-wire probes. Journal of Fluid Mechanics 219, 119–142.

Klewicki, J., Falco, R., 1996. Spanwise vorticity structure in turbulent boundary layers. International Journal of Heat and Fluid Flow 17, 363–376.

Marusic, I., Uddin, A., Perry, A., 1997. Similarity law for the streamwise turbulence intensity in zero-pressure-gradient turbulent boundary layers. Physics of Fluids 9, 3718–3726.

McKeon, B., Li, J., Jiang, W., Morrison, J., Smits, A., 2004. Further observations on the mean velocity distribution in fully-developed pipe flow. Journal of Fluid Mechanics 501, 135–147.

Metzger, M., 2002. Scalar dispersion in high Reynolds number turbulent boundary layers. Ph.D. thesis, University of Utah, Salt Lake City, Utah.

Metzger, M.M., Klewicki, J.C., 2001. A comparative study of near-wall turbulence in high and low Reynolds number boundary layers. Physics of Fluids 13, 692–701.

Metzger, M., Klewicki, J., 2003. Development and characterization of a probe to measure scalar transport. Measurement Science Technology 14, 1437–1448.

Metzger, M.M., Klewicki, J.C., Bradshaw, K., Sadr, R., 2001. Scaling the near-wall axial turbulent stress in the zero pressure gradient boundary layer. Physics of Fluids 13, 1819–1821.

Metzger, M., Klewicki, J., Priyadarshana, P., 2003. Reynolds number dependencies in the behavior of boundary layer axial stress and scalar transport. In: Smits, J.A. (Ed.), Reynolds Number Scaling in Turbulent Flows. Kluwer Academic Publishers, pp. 83–89.

Nagano, Y., Tsuji, T., Houra, T., 1998. Structure of turbulent boundary layer subjected to adverse pressure gradient. International Journal of Heat and Fluid Flow 19, 563–572.

Osterlund, J., Johansson, A., Nagib, H., Hites, M., 2000. A note on the overlap region in turbulent boundary layers. Physics of Fluids 12, 1–4.

Perry, A., Abell, C., 1975. Scaling laws for pipe-flow turbulence. Journal of Fluid Mechanics 67, 257–271.

Perry, A., Abell, C., 1977. Asymptotic similarity of turbulence structures in smooth-and rough-walled pipes. Journal of Fluid Mechanics 79, 785–799.

Tennekes, H., Lumley, J.L., 1972. A First Course in Turbulence. The MIT Press, Cambridge, Massachusetts.

Townsend, A., 1976. The Structure of Turbulent Shear Flow, second ed. Cambridge University Press, Cambridge.